Am J Transl Res 2019;11(12):7523-7537
www.ajtr.org /ISSN:1943-8141/AJTR0100895

Original Article

Visual deprivation modifies glutamate receptor expression in visual and auditory centers

You Zhou[1,2,3], Manli Yin[4], Chenchen Xia[4], Xueling Wang[1,2,3], Hao Wu[1,2,3], Yonghua Ji[4,5]

[1]Department of Otolaryngology-Head and Neck Surgery, Ninth People's Hospital, Shanghai Jiaotong University School of Medicine, Shanghai 200011, China; [2]Ear Institute, Shanghai Jiaotong University School of Medicine, Shanghai 200125, China; [3]Shanghai Key Laboratory of Translational Medicine on Ear and Nose Diseases, Shanghai 200125, China; [4]Institute of Biomembrane and Biopharmaceutics, Shanghai University, Shanghai 200444, China; [5]Translational Institute for Cancer Pain, Xinhua Hospital Chongming Branch, Shanghai 202150, China

Received August 13, 2019; Accepted December 7, 2019; Epub December 15, 2019; Published December 30, 2019

Abstract: Changes in the electrical activities of visual and auditory thalamic-cortical regions account for the cross-modal enhancement of auditory perception following visual deprivation, but the molecular regulatory factors mediating these changes remain elusive. In this study, we showed that the expression patterns of five glutamate receptor (GluR) subunits which involved in regulating the synaptic plasticity in mouse primary visual (V1) cortex and primary auditory (A1) cortex undergone elaborate modification with layer-specificity after visual deprivation using dark-exposure (DE). The expression levels of NR1 and NR2B were increased, and those of GluR1 and NR2B in the V1 cortex were decreased after DE. In the A1 cortex, the expression levels of NR1, NR2A and NR2B were increased, and the expression levels of GluR1 and GluR2 were decreased after DE. The altered expression levels of GluR subunits selectively happened in the different layers of V1 and A1 cortices. In addition, the expression level of GluR2 in lateral geniculate nucleus (LGN) was decreased. These results provide novel molecular clues for the plastic neural activity in visual and auditory centers in the absence of visual input, and hint the extensive refinement of intracortical circuits and thalamocortical feedback circuits underlying the multisensory cross-modal plasticity.

Keywords: Visual deprivation, cross-modal plasticity, oscillation, glutamate receptor

Introduction

Blind individuals often display better tactile acuity [1], sound localization [2, 3], pitch discrimination [4] and odor identification [5, 6] than sighted individuals. There is a growing consensus that the central nervous system is able to adapt to the loss of one modality, including reorganization in the sensory-deprived cortex to process the spared senses and adaptive plasticity in the remaining sensory cortices, which is termed as the cross-modal plasticity [7-9]. Sensory cortices have a laminar architecture (layer I, II/III, IV, V, and VI), each layer presents specific function in information processing [10]. Recent studies in rodents have revealed that dark-exposure (DE) can lead to the reinforcement of excitatory synapses in the layer II/III of V1 cortex, the increased amplitude of miniature excitatory postsynaptic currents (mEPSCs) returns to normal level after re-exposure to light [11]. Monocular enucleation can reduce the neural activity in the deprived monocular zone of V1 cortex, while the decreased activity returns to normal levels after whisker stimulation [12, 13]. In contrast, DE decreases the excitatory synaptic transmission in the layer II/III of S1 (primary somatosensory cortex) and A1 cortices [8, 11]. DE also produces distinct changes of the thalamocortical connections in the spared and deprived sensory cortices, shifting between feedforward and intracortical processing to allow adaptation [14]. For example, DE strengthens thalamocortical synapses in layer IV of A1 but not in V1 cortex, whereas deafening potentiates thalamocortical synapses in layer IV of V1, but not in A1 cortex [15]. These findings demonstrate the plastic adaptation of neural activity in spared and deprived sensory thalamic-cortical areas in the absence of one sensory modality.

It is well known that synapse transmission is the fundamental procedure of neural informa-

tion conduction. The α-amino-3-hydroxy-5-methyl-4-isoxazole-propionic acid (AMPA) receptor and N-methyl-D-aspartic acid (NMDA) receptor at a majority of excitatory synapses in central system are important regulatory factors of synaptic plasticity. Neurons regulate the synaptic activity and transmission efficiency by modifying the number, distribution and composition of GluR subunits, which is called synaptic plasticity [16]. However, little is known about the GluRs contributing to the cross-modal plasticity. The goal of the present study was to investigate how the expression patterns of GluRs change in mouse visual and auditory centers in the absence of vision input.

Materials and methods

Animals and visual manipulation

Male C57BL6J mice were obtained from SLAC Laboratory Animal Co., Ltd (Shanghai, China) and maintained in a light-permeable cage (26.5 cm * 16 cm * 14 cm) with standard food and water provided *ad libitum*. Visual deprivation model was created by exposing mice (postnatal day (P) 21) to complete darkness for 7 days (P28, the DE group). Control animals were mice of a same age and strain exposed to a normal visual experience with a 12/12 h light/dark cycle (P28, the NR group) [15]. The experimental procedures (Figure S1) described here were performed in accordance with the National Institutes of Health (NIH) guidelines for the Care and Use of Laboratory Animals and were approved by the Ethics Committee and the Committee of Animal Experimentation at Shanghai University.

Local field potential (LFP) recording

NR and DE mice (P28) were anesthetized with chloral hydrate (10%, 4.5 mL/kg) and ethyl carbamate (20%, 2 mL/kg), placed in a stereotaxic frame and implanted with a 16-channel nickel-chromium microelectrode array (impedance less than 1 MΩ). Electrodes were placed in the layer II/III of A1 cortex (3.2 mm posterior to bregma, 4.4 mm lateral to midline, 0.35 mm below the brain surface), and the layer II/III of V1 cortex respectively (3.1 mm posterior to bregma, 2.2 mm lateral to midline, 0.35 mm below the brain surface), according to brain topography. Recordings of LFP were performed in the absence of visual or acoustic stimuli in a dark and sound-attenuated cubicle (with background noise level at approximately 30 dB). To reduce various interferences of ambient electromagnetic fields, the recording chamber was placed in a Faraday cage. LFPs were acquired as broadband signals (0.1 Hz~5 kHz) using an OmniPlex System (Plexon Inc., Dallas, TX, USA). Then, the brains were sliced and stained using Nissl method to permit the localization of electrodes. The following data analyses were performed off-line with custom-written MATLAB scripts. The raw data were imported into the MATLAB environment, and a random 10 s epoch in each recording was selected and extracted to a single file. LFP recordings were low-pass filtered with a cutoff at 300 Hz. Line noise artifacts were removed using a 50 Hz Butterworth notch filter. Power spectral density (PSD) was computed using the Welch technique, with Hamming windowing and a fast Fourier transform segment length of 512 samples with a 256-sample overlap. Changes in the power of five frequency oscillations (δ: ~1-4 Hz, θ: ~4-8 Hz, α: ~8-13 Hz, β: ~13-30 Hz, γ: ~30-90 Hz) were analyzed. Wavelet packet decomposition was used to extract the five frequency bands. The power of each oscillation was computed separately. The "n" represents the mouse number recorded successfully in each accurate area of two groups (one NR mice and three DE mice were excluded herein because of improper placement).

Real-time quantitative PCR (qPCR)

NR and DE mice (P28; n=14, n=15, respectively) were anesthetized with chloral hydrate (10%, 4.5 mL/kg) and decapitated. The brain blocks of NR and DE mice containing the V1, A1, LGN and MGB were removed respectively. Coronal slices (200 μm) were cut with a vibrating slicer (VT-1000S; Leica, Nussloch, Germany) in ice-cold artificial cerebral spinal fluid (ACSF) containing the following (in mmol/L): 124 NaCl, 5 KCl, 2.4 $CaCl_2$, 1.3 $MgSO_4$, 1.2 KH_2PO_4, 26.2 $NaHCO_3$ and 10 glucose (pH 7.4, 308 mOsm/L, 95% O_2 saturated). The four samples (V1, A1, LGN, and MGB) were separated by syringe needle and gathered in liquid nitrogen. Total RNA was extracted using Trizol (Sangong Biotech, Shanghai, China) according to the manufacturer's protocol. The synthesis of first-strand cDNA and qPCR was performed using PrimeScript RTase and SYBR Premix ExTaq Kit (Takara, Dalian, Hebei, China). Primers were synthesized by Genscript (Nanjing, Jiangsu, China) and the sequences of them were listed in Table S1.

The relative expression levels for the glutamate receptor transcripts were calculated by the $2^{-\Delta\Delta CT}$ method. The expression levels of five glutamate receptors (GluRs) were normalized using β-actin as endogenous controls. Each experiment was repeated four to six times, with three independent cDNA samples. The "n" value represents the number of normalized values.

Western blotting

The V1 and A1 samples of NR (n=30, 10 mice per independent sample) and DE (n=30, 10 mice per independent sample) mice were separately collected. Homogenate protein extraction was performed using RIPA Lysis buffer according to the manufacturer's protocol (Weiao Biotech, Shanghai, China). Protein concentrations were measured using a BCA Protein Quantification Kit (Yeasen, Shanghai, China) with a microplate reader (Bio-Rad, Hercules, CA, USA). Protein fractions were separated by SDS-PAGE and transferred to PVDF membranes (0.45 μm; Millipore, Billerica, MA, USA). Membranes were blocked with blocking solution (5% non-fat dried skimmed milk powder, 0.01 M phosphate buffer solution (PBS), 0.1% Tween-20) at temperature for 2 h, subsequently incubated with primary antibody overnight at 4°C, and finally incubated with secondary antibody for 2 h at room temperature. Primary antibodies: rabbit polyclonal to GluR1 (1:200; Santa Cruz, San Francisco, CA, USA), rabbit monoclonal to GluR2 (1:1000; Abcam, Cambridge, MA, USA), rabbit polyclonal to NR1 (1:200; Santa Cruz), rabbit polyclonal to NR2A (1:200; Santa Cruz), rabbit polyclonal to NR2B (1:200; Abcam), mouse monoclonal to β-actin (1:1000; Abcam). Secondary antibodies: Goat anti-rabbit IgG-HRP (1:8000; Santa Cruz), Goat anti-mouse IgG-HRP (1:10000; Santa Cruz). The blots were visualized by incubating with enhanced chemofluorescent reagent ECL (WBKLS0050; Millipore, Billerica, MA, USA) with automatic chemiluminescence image analysis system (Tanon-5200; Tanon Science & Technology Co., Ltd, Shanghai, China). These experiments were performed at least three times, the gray value of protein bands were quantitatively analyzed using Image analysis software (Image-Pro plus 6.0; National Institutes of Health, Bethesda, MD, USA). The "n" value represents the number of blot band for data analysis.

Immumohistochemical staining

NR and DE mice (P28; n=9, n=9, respectively) were deeply anesthetized and perfused with sterile saline and 4% paraformaldehyde in 0.1 M PBS (pH 7.4). Brains were removed and fixed using 4% paraformaldehyde for two days, and then were placed in 20% and 30% sucrose for dehydration. Serial coronal series sections (20 μm) were collected using a freezing microtome (HM525; Microm, Walldorf, Germany) and mounted on glass slides. Brain sections were washed three times with PBS for 5 min each and incubated in 0.5% Triton X-100 including 3% H_2O_2, for 30 min at room temperature. After washing with PBS, samples were antigen-retrieved for 25 min with pepsin at 37°C. Next, samples were washed three times and blocked for 1 h with 5% goat albumin serum at room temperature. Primary antibodies against GluR1 (1:50; Santa Cruz), GluR2 (1:500; Abcam), NR1 (1:100; Santa Cruz), NR2A (1:50; Santa Cruz), and NR2B (1:200; Abcam) were diluted in 5% goat serum. After incubation at 4°C for 24 h, samples were washed three times in PBS and incubated with biotin-conjugated goat anti-rabbit immunoglobulin G (Weiao Biotech) at room temperature for 30 min. Samples were again washed, and developed using the chromagen 3, 3'-diaminobenzidene, 5% diluted with PBS and 0.1% H_2O_2, for 8 minutes. Samples were dehydrated, cover-slipped and photographed using an upright microscope (Nikon, Sendai, Japan). The primary cortex (including layer I-VI, shown in Figure S2) of each slice was chosen according to the rat brain topography. The average optical density (Integrated Optical Density (IOD)/area) of three randomly selected, non-overlapping fields was assessed using Image-Pro Plus software. One or two slices of each cortex from each individual mouse were selected for one GluR subunit staining. The "n" described in the results represents the number of V1 or A1 slices used for data collection in each experiment.

Transcriptome

The LGN and MGB samples of NR and DE mice were separately collected. Four cDNA libraries of LGN samples respectively from NR (n=24, 12 mice per independent LGN sample) and DE (n=22, 11 mice per independent LGN sample) mice (NR-LGN-1, NR-LGN-2, DE-LGN-1, DE-LGN-2) and four cDNA libraries of MGB samples

respectively from NR (n=20, 10 mice per independent MGB sample) and DE (n=24, 12 mice per independent MGB sample) mice (NR-MGB-1, NR-MGB-2, DE-MGB-1, DE-MGB-2) were constructed according to Illumina's instructions (Shanghai Personalbio Co., China). The mRNA was isolated using magnetic oligo (dT) beads. Fragmentation buffer was added to cleave the mRNA into short fragments, and these fragments were used as templates. Random hexamer-primers were used to synthesize first-strand cDNA. Buffer, dNTPs, RNase H, and DNA polymerase I were used to synthesize second-strand cDNA. Then, the fragments were purified using a QiaQuick PCR extraction kit (Qiagen, Hilden, Germany) and resolved with elution buffer for end repair and poly (A) addition. The resulting short fragments were then connected to sequencing adapters. Fragments with a suitable range of lengths were selected based on the results of agarose gel electrophoresis and were used as templates for library amplification. Library quantification was performed using Pico green and a fluorescence spectrophotometer (Quantifluor-ST fluorimeter, Promega; Quant-iT Pico Green dsDNA Assay Kit, Invitrogen). These libraries were pair-end sequenced using Illumina NextSeq 500. Raw data generated by sequencing were stored in fastq format and submitted to the National Center for Biotechnology Information Sequence Read Archive SRA database (accession number: PRJNA505943).

Raw sequencing data were filtered to remove low-quality reads before subsequent analysis. Quality analysis by means of FastQC showed that the average quality of the filtered data was very high. Theoretical values coincided well with the measured values (Table S2). To annotate all useful reads, the clean reads were mapped to the mouse genome database, and RPKM (reads per kilo base per million reads) values were used to measure the expression of each gene. The DESeq package was adopted to estimate variance-mean dependence in the count data from the Illumina sequencing assays and to test for differential expression based on a model using the negative binomial distribution in accordance with equation (1): (1) v=sμ+αs2μ2, where m is the expected normalized count value (estimated by the average normalized count value), s is the size factor for the sample under consideration, and α is the dispersion value for the unigene. Differentially-expressed genes were detected in NR and DE samples based on average expression levels that differing at least a 1.5-foldchange and *P*-values < 0.05 when comparing NR and DE samples. At the same time, RPKM >0.1 was set to the impersonal expression. The pathway assignments were carried out by sequence searches against Kyoto Encyclopedia of Genes and Genomes (KEGG) database.

Statistical analysis

Data are presented as the mean ± SEM and were analyzed using Graphpad Prism 7 (GraphPad Software, La Jolla, CA, USA). The differences between the two groups (NR and DE) were compared using an unpaired Student's two-tailed t-test. $P < 0.05$ was considered to be statistically significant. The investigators who performed the data acquisition and quantification were blind to the experimental conditions.

Results

DE changes LFP oscillations in the V1 and A1 cortices

LFP recordings *in vivo* showed that the raw LFP traces in the layer II/III of V1 and A1 cortices were altered in the DE group (**Figure 1A** and **1E**). After the raw traces were extracted into five frequency bands, the PSD was found to be embellished across different frequency bands after DE (**Figure 1C**, **1D**, **1G** and **1H**). The total power of raw LFP oscillations in the V1 cortex was markedly increased (by 62.79%, $P < 0.01$) in the DE group compared to that in the NR group (NR, n=6 mice; DE, n=6 mice). The power of high-frequency γ oscillation in the V1 cortex was significantly enhanced after DE (by 45.83%, $P < 0.01$). The power of low-frequency δ oscillation in V1 were remarkable larger in the DE group than in the NR group (by 200.00%, $P < 0.001$). The power of another low-frequency θ oscillation was decreased in V1 after DE (by 51.52%, $P < 0.001$) (**Figure 1B**). In the A1 cortex, the total power of raw LFP oscillations was obviously increased (by 76.73%, $P < 0.001$) in the DE group compared to that in the NR group (NR, n=6 mice; DE, n=6 mice). In contrast to V1 cortex, the power of γ oscillation was decreased after DE (by 56.10%, $P < 0.05$). In addition, the power of α oscillations was similarly decreased (by 60.00%, $P < 0.001$), whereas the θ power was significantly increased after DE (by 343.96%, $P < 0.001$) (**Figure 1F**).

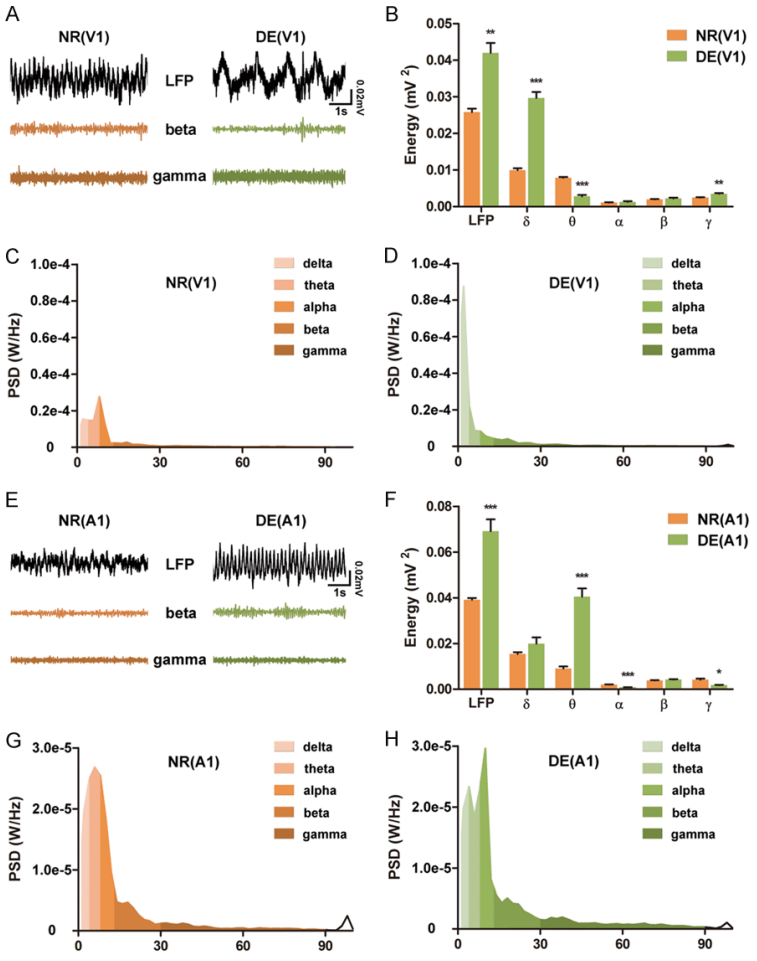

Figure 1. Changes in LFP characteristics in the V1 and A1 cortices after DE. A. Random LFP segments recorded in the V1 cortices of NR and DE mice alone with β and γ oscillations extracted from these segments. B. The power of five oscillations of LFP from the V1 cortices is shown in the bar graph (mV^2). C, D. Average PSD from the V1 cortices is shown after it was normalized and computed with fast Fourier transform (FFT). Each bar graph was painted into five areas in order to distinguish one oscillation from the others. E. Random LFP segments from the A1 cortices of NR and DE mice alone with β and γ oscillations extracted from these segments. F. The power of five oscillations from the A1 cortices is shown in the bar graph (mV^2). G, H. Average PSD from the A1 cortices is shown after it was normalized and computed with FFT. Data are shown as the mean ± SEM. Asterisks indicate levels of significance determined by unpaired Student's two-tailed t-test with statistical significance at *P < 0.05, **P < 0.01 and ***P < 0.001.

DE modifies expression patterns of GluRs in the V1 and A1 cortices

To pinpoint the molecular clues underlying the changed neural activity in the V1 and A1 cortices following DE, the expression levels of five GluRs were analyzed. The qPCR experiments showed that the mRNA level of NR1 (P < 0.001; NR n=12, DE n=12) and NR2B (P < 0.01; NR n=12, DE n=12) were markedly increased in the V1 cortex of DE group, and the mRNA levels were decreased for both GluR1 (P < 0.001; NR n=18, DE n=18) and NR2A (P < 0.01; NR n=12, DE n=12) in the V1 cortex of DE group. Western blot experiments showed that the protein levels of NR1 (P < 0.001; NR n=8, DE n=8) and NR2B (P < 0.05; NR n=13, DE n=13) were significantly increased in the V1 cortex of DE group, whereas the protein levels of GluR1 (P < 0.05; NR n=7, DE n=7) and NR2A (P < 0.01, NR n=6, DE n=6) were decreased in the V1 cortex of DE group. By immunohistochemical staining, it was found that the expression level of NR1 was up-regulated in the layer II/III (P < 0.05) and layer IV (P < 0.05) of V1 cortex (NR n=9, DE n=9), while the expression level of NR2B was up-regulated in the layer IV (P < 0.05), V (P < 0.01), and VI (P < 0.01) of V1 cortex after DE (NR n=9, DE n=9). On the other hand, the expression level of GluR1 was down-regulated in the layer I (P < 0.05), IV (P < 0.01) and V (P<0.01) of V1 cortex (NR n=9, DE n=9), the expression level of NR2A was only down-regulated in the layer IV of V1 cortex (P < 0.05; NR n=9, DE n=9). Moreover, the expression level of GluR2 was significantly increased in the layer V of V1 cortex (P < 0.05; NR n=9, DE n=9), although the changes of GluR2 mRNA and protein cannot be detected in the intact V1 cortex after DE (**Figure 2**).

In the A1 cortex, the mRNA levels of GluR1 (P < 0.01; NR n=18, DE n=18) and GluR2 (P < 0.01; NR n=18, DE n=18) were decreased, and the mRNA levels of NR1 (P < 0.01; NR n=12, DE n=12), NR2A (P < 0.01; NR n=12, DE n=12) and NR2B (P < 0.01; NR n=12, DE n=12) were increased after DE. The protein expression levels of GluR1 (P < 0.05; NR n=6, DE n=6) and GluR2 (P < 0.05; NR n=7, DE n=7) were decreased, and the protein expression levels of NR1 (P < 0.01; NR n=6, DE n=6), NR2A

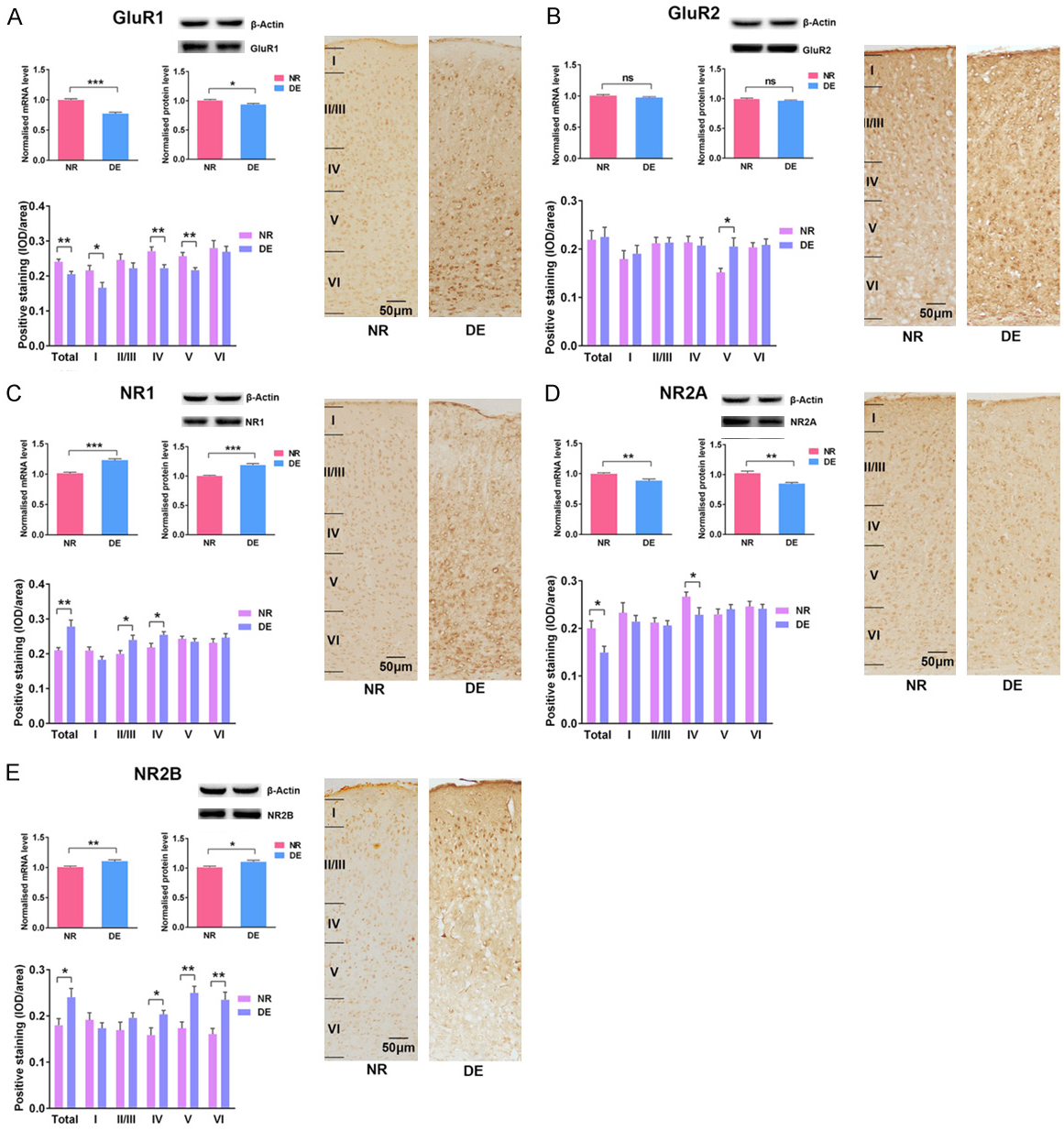

Figure 2. Dynamic expression patterns of GluRs in the V1 cortex after DE. A. GluR1 expression in the V1 cortices from NR and DE mice. Bar graph (Left upper-left) shows the mRNA level of GluR1 by normalizing against the mean of β-actin. Bar graph (Left upper-right) shows the protein level of GluR1, data are presented with IOD/area and are normalized to NR control. Bar graph (Left-bottom) shows the IOD/area quantification of GluR1 in five layers (I, II/III, IV, V, and VI) of the V1 cortex. The representative immunohistochemical labeling (Right) shows the GluR1 protein expression profiles in the V1 cortices from NR and DE mice. B-E. They show the expression patterns of other four subunits (GluR2, NR1, NR2A, and NR2B), with the same arrangement mode. Data are shown as the mean ± SEM. Asterisks indicate levels of significance by unpaired Student's two-tailed t-test with statistical significance at *P < 0.05, **P < 0.01 and ***P < 0.001.

(P < 0.05; NR n=10, DE n=10) and NR2B (P < 0.05; NR n=8, DE n=8) were increased in the A1 cortex of DE group. By layer-staining analysis, it was found that the expression level of GluR1 was down-regulated in the layer II/III (P < 0.05) and layer IV (P < 0.05) of A1 cortex (NR n=9, DE n=9), and the expression level of GluR2 was down-regulated in the layer II/III (P < 0.05)

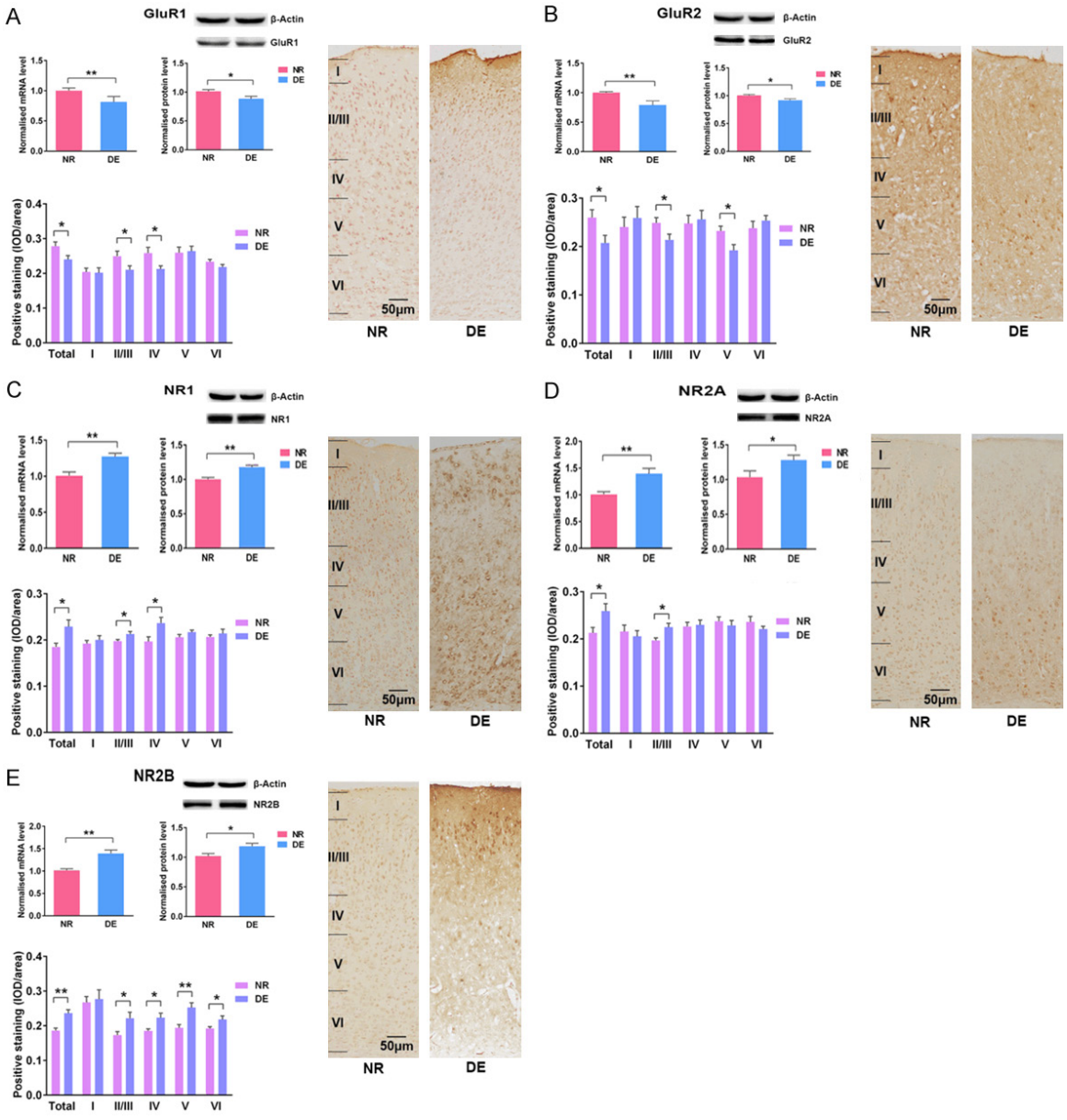

Figure 3. Dynamic expression patterns of GluRs in the A1 cortex after DE. A. GluR1 expression in the A1 cortices from NR and DE mice. Bar graph (Left upper-left) shows the mRNA level of GluR1 in A1 by normalizing against the mean of β-actin. Bar graph (Left upper-right) shows the protein level of GluR1, data are normalized to NR control. Bar graph (Left-bottom) shows the IOD/area quantification of GluR1 in five layers (I, II/III, IV, V, and VI) of the A1 cortex. The representative immunohistochemical labeling (Right) shows the GluR1 protein expression profiles in the A1 cortices from NR and DE mice. B-E. They show the expression patterns of other four subunits (GluR2, NR1, NR2A, and NR2B), with the same arrangement mode. Data are shown as the mean ± SEM. Asterisks indicate levels of significance by unpaired Student's two-tailed t-test with statistical significance at *P < 0.05, **P < 0.01 and ***P < 0.001.

and layer V (P < 0.05) of A1 cortex after DE (NR n=9, DE n=9). On the other hand, the expression level of NR1 was increased in the layer II/III (P < 0.05) and layer IV (P < 0.05) of A1 cortex (NR n=9, DE n=9), the expression level of NR2A was only increased in the layer II/III of A1 cortex after DE (P < 0.05; NR n=9, DE n=9). The expression level of NR2B presented with widely rising tendency in four different layers of the A1 cortex after DE, except layer I (P < 0.05, P < 0.05, P < 0.01, P < 0.05 respectively; NR n=9, DE n=9) (**Figure 3**).

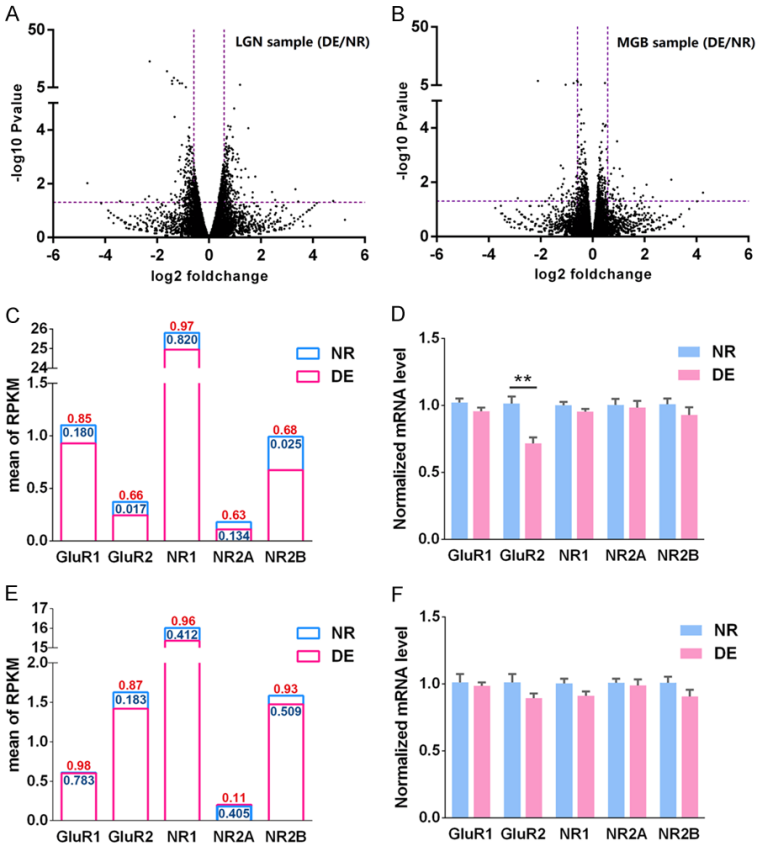

Figure 4. Changed expression levels of GluRs in the LGN and MGB after DE. A. Volcano plot of the expression levels of genes in NR-LGN and DE-LGN. B. Volcano plot of the expression levels of genes in NR-MGB and DE-MGB (y-axis, $\log_{10}$ *P*-value of difference; x-axis, $\log_2$ fold-changes; fold-change ≥1.5, *P*-value < 0.05 and RPKM value >0.1 were set as threshold to identify differentially-expressed genes). C. Average RPKM values of five GluRs in LGN (the numerical value in blue and red respectively signify the *P*-value and fold-change value). D. The expression levels of five GluRs in LGN were verified by qPCR. Data are shown as the mean ± SEM. Asterisks indicate levels of significance by unpaired Student's two-tailed t-test with statistical significance at **P < 0.01. E. The average RPKM values of five GluRs in MGB. F. The expression levels of five GluRs in MGB were verified by qPCR.

DE alters gene expression patterns in the LGN and MGB

Our previous study has revealed that oscillatory activities in thalamic LGN and MGB were profoundly modified in the absence of visual input [17]. Here, transcription expression profile was employed to detect the differentially-expressed gene which may be involved in the altered neural electrical activity in LGN and MGB following DE. It was found that 380 differential expression genes were detected in the LGN of DE group, among them, the expression levels of 203 genes were up-regulated and those of 177 genes were shown as down-regulated tendency (**Figures 4A**, **5** and **6**). By KEGG pathway analysis, it was revealed that the differential expression genes were mainly involved in the process of protein synthesis and oxidative phosphorylation (**Figure 8**). On the other hand, 46 differential expression genes were detected in the MGB after DE, including 22 up-regulated genes and 24 down-regulated genes (**Figures 4B** and **7**). Furthermore, these differential expression genes were mainly related to signal transduction pathways, such as PI3K-Akt, Wnt and TNF (**Figure 8**). Focusing on GluRs expression, it was showed that the expression level of GluR2 in LGN of DE group was significantly down-regulated, which was verified by qPCR ($P < 0.01$) (**Figure 4C** and **4D**). The expression levels of five GluR subunits were no detectable change in the MGB of DE group (**Figure 4E** and **4F**).

Discussion

Refinement of intracortical and thalamocotical circuits following DE

LFP oscillations are often accompanied by synchronization of activity in a widespread cerebral area and deemed to have a common mechanism underlying neuronal assembly formation [18]. The present study found that oscillations in the layer II/III of mice V1 cortex undergone remarkable amendment in the absence of visual input. The enhancement of raw LFP oscillations and high-frequency γ oscillation suggests that neural excitability in the layer II/III of V1 cortex was increased after DE. This result is consistent with a previous report showing the increased amplitude of mEPSCs of pyramidal neurons in the layer II/III of V1 cortex after DE [11]. In addition, the high-frequency β and γ oscillations in the layer IV of V1 cortex were also enhanced after visual deprivation

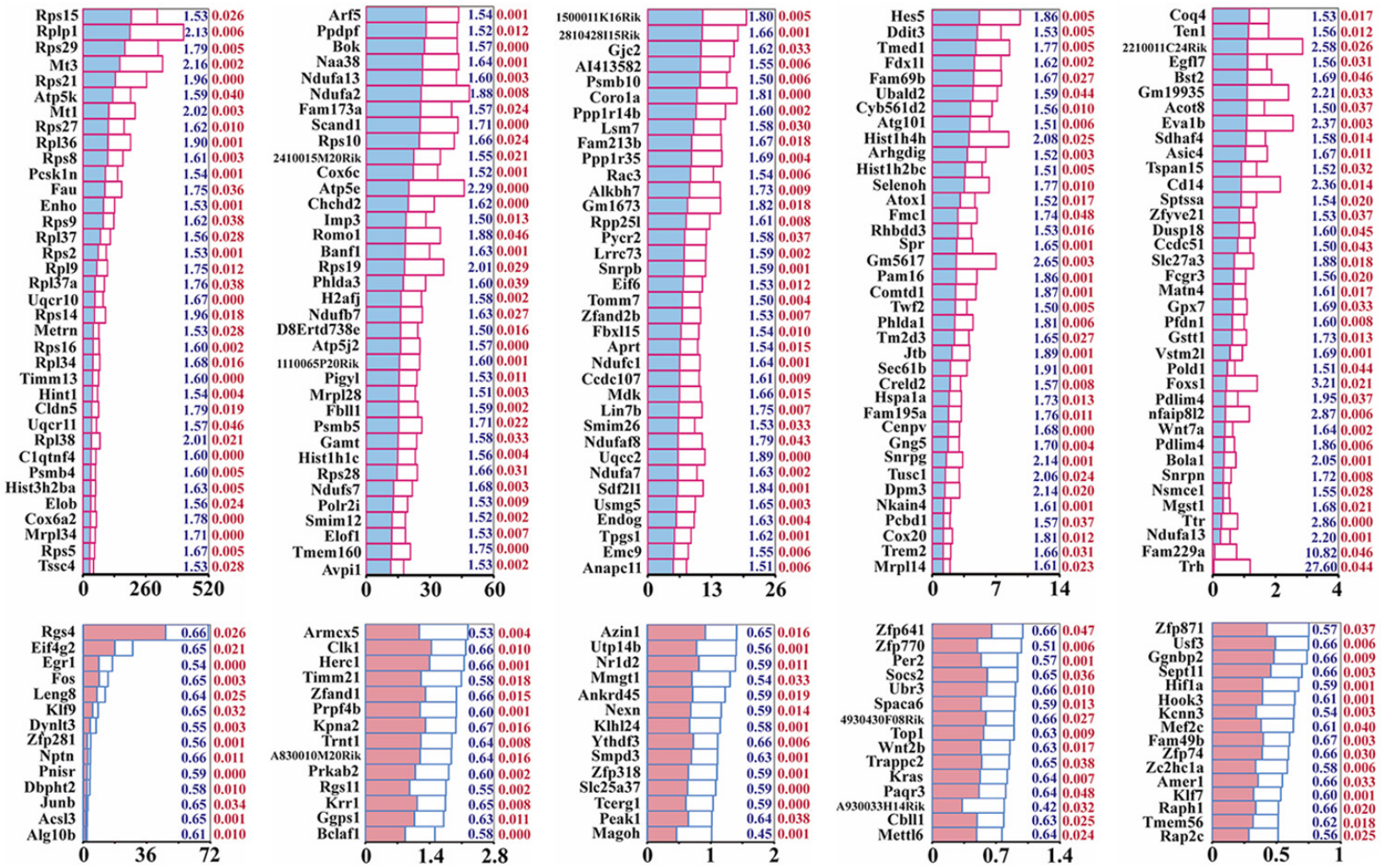

Figure 5. Differentially-expressed genes (RPKM value >0.5) in the NR-LGN and DE-LGN. Average RPKM values of differentially-expressed genes from NR and DE mice were shown with blue column/red line (182 genes, up-regulation) and red column/blue line (73 genes, down-regulation), respectively. The numerical value in blue on the right represent the fold-change value (DE versus NR), the numerical value in red on the right signify the *P*-value.

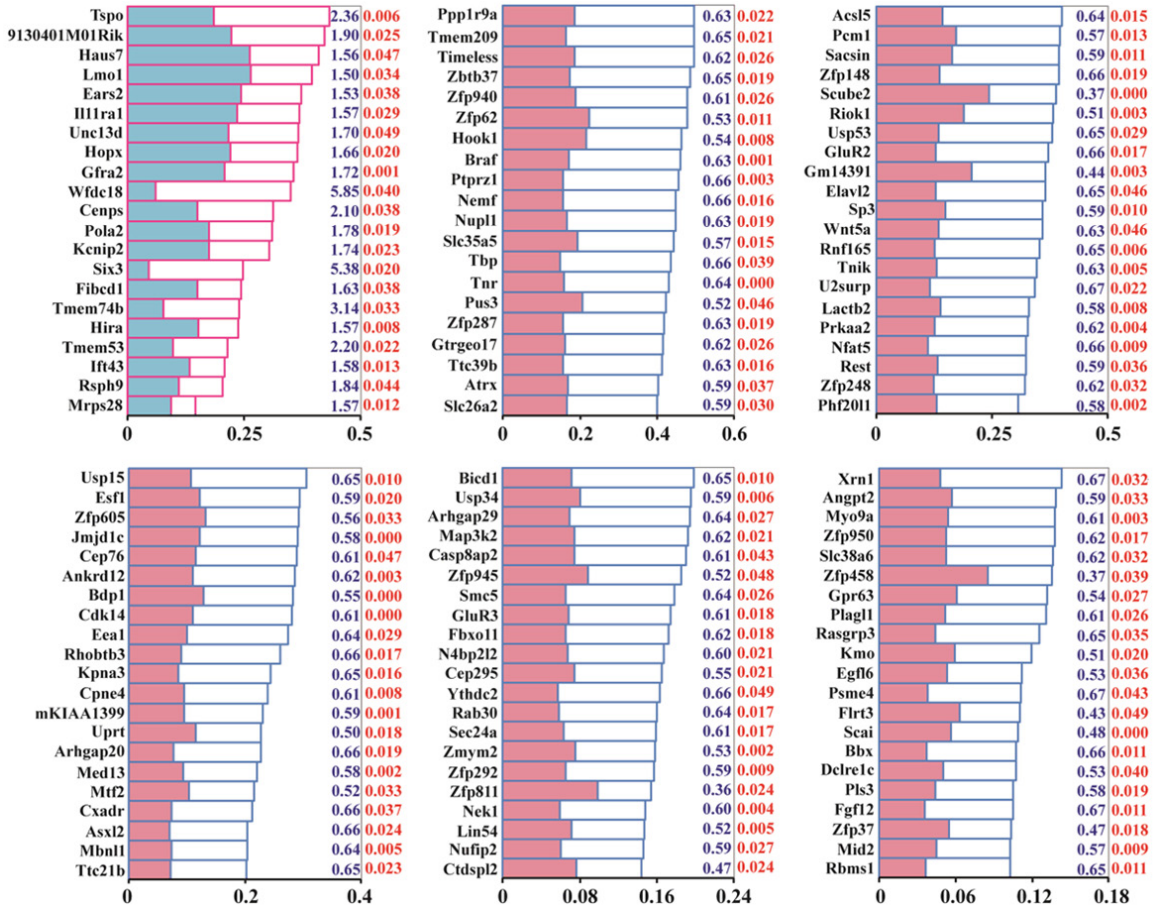

Figure 6. Differentially-expressed genes (0.1 < RPKM value < 0.5) in NR-LGN and DE-LGN. Average RPKM values of differential expression genes from NR group and DE group were shown with blue line/column (21 genes, up-regulation) and red line/column (104 genes, down-regulation), respectively. The numerical value in blue on the right represent the fold-change value (DE versus NR), the numerical value in red on the right signify the *P*-value.

[17]. These data indicate that the cellular excitation in the V1 cortex is globally strengthened for processing other remaining senses when visual input is lacking. On the other hand, the present study showed that the power of high-frequency γ oscillation was reduced, which suggests that neural excitability in the layer II/III of A1 cortex was decreased after DE. The weakened neural electrical activity could be attributed to the decreased amplitude of mEPSCs of pyramidal neurons in the layer II/III of A1 cortex after DE [11]. It is noted that LFP oscillations in the layer IV of A1 cortex was markedly enhanced [17], the strength of thalamocortical synapses projecting from MGB to the layer IV of A1 cortex was increased after DE [15]. These results suggest that the A1 cortex is undergone plastic regulation following DE, in addition to the adaptation of the V1 cortex. Besides, the low-frequency rhythms (δ, θ and α oscillation) in the V1 and A1 cortices were also varied after DE. However, the roles of low-frequency rhythms in cortices involved in sensory perception need to be further defined [19, 20]. Taken together, the extensive and distinct variation of neural activities in the layer II/III and IV of V1 and A1 cortices during the absence of visual input suggest that, the elaborate refinement of intracortical circuits and the fine adjustment of thalamocortical connections maybe the basis of the cross-modal plasticity.

Dynamic expression of GluRs in the V1 and A1 cortices after DE

The AMPARs and NMDARs are major ionotropic glutamate receptors that respond to physiological glutamate, the combined accumulation and dynamic expression of GluRs within synapses is important for induction and maintainence

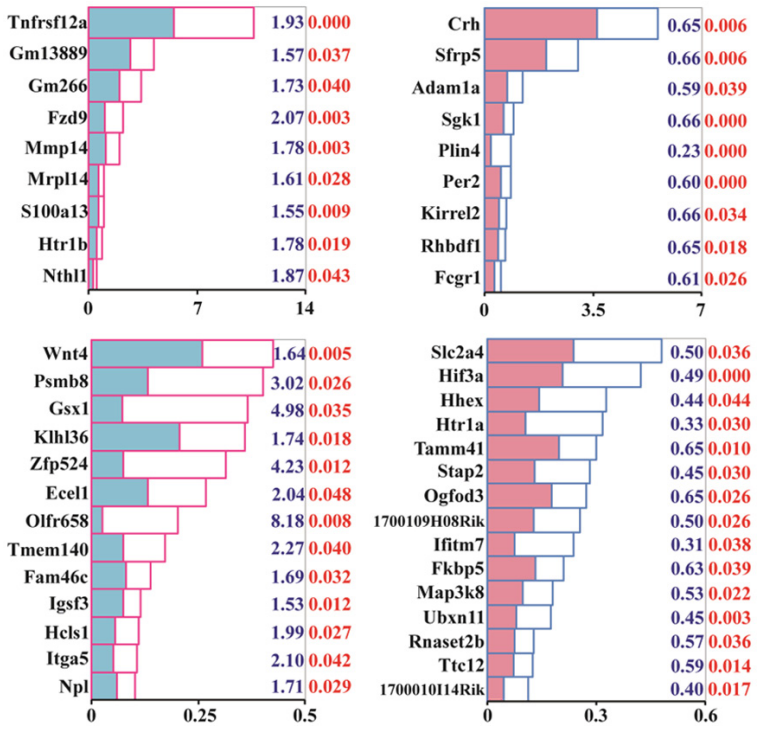

Figure 7. Differentially-expressed genes in NR-MGB and DE-MGB. The expression value of differential expression genes from NR group and DE group were shown with blue column and red column, respectively. Numbers in blue signify the fold-change value, numbers in red signify the *P*-value. 9 genes (RPKM >0.5) and 13 genes (0.1 < RPKM < 0.5) were presented with higher expression levels in DE-MGB samples. 9 genes (RPKM >0.5) and 15 genes (0.1 < RPKM < 0.5) were presented with higher expression levels in DE-MGB samples.

of synaptic plasticity [21, 22]. AMPA receptors include four subunits (GluR1-GluR4), and the combination of each subunit forms a distinct receptor complex in the mammalian central nervous system, mature neurons usually express GluR1/GluR2 heterotetrameric receptors [23]. The present study found that the expression level of GluR1 were down-regulated in total homogenate of the V1 cortex after DE (from P21 to P28), but not in the case of GluR2. The down-regulation of GluR1 in the V1 cortex herein seems to be inconsistent with a previous study [11], the discrepant results may be attributed to the different DE time-window in the two studies. The expression levels of GluR1 and GluR2 in total homogenate of the A1 cortex were both down-regulated after DE found in the present study, which hint the diverse of synaptic plasticity between the V1 and A1 cortices in the absence of visual input. NMDA receptor is a heteromer that contains an obligatory NR1 subunit and a mixture of NR2A-D subunits [24, 25]. The present study revealed that the expression levels of NR1 and NR2B were up-regulated, in contrast, that of NR2A was down-regulated in total homogenate of the V1 cortex after DE. The result is in accordance with previous reports (the lower NR2A/2B ratio in the V1 cortex by visual deprivation attributing to a reduction in NR2A and an elevation of NR2B level) [26, 27]. Interestingly, the expression levels of NR1, NR2B and NR2A in total homogenate of the A1 cortex were both increased after DE found in the present study, which strongly suggest that NMDARs may be the indispensable molecular regulatory factors accounting for the enhanced electrical activity in the A1 cortex.

Layer-specific variation of GluRs expression in the V1 and A1 cortices after DE

Sensory cortices have a laminar architecture including six layers (Layer I, II/III, IV, V, VI), the structural characteristics and physiological functions of each layer are diverse [28, 29]. Sensory information is believed to propagate through the cortical column along the layer IV→II/III→V/VI pathway. Layer V neurons comprise a major output of the cortex with the most substantial axonal innervation of subcortical and cortical structures, layer VI neurons transmit feedback to thalamus and cortex [30]. As shown in **Figure 9**, the expression patterns of AMPARs and NMDARs in the different layers of the primary cortices were found to be delicately modified in the present study.

The present study found that the expression level of GluR1 in the layer IV of V1 cortex was decreased, accompanied by constant expression level of GluR2 after DE. However, this result seems to be hard to explain the constant amplitude of AMPA-mediated mEPSCs in the layer IV of V1 cortex after visual deprivation [15]. It is well known that phosphorylation can regulate the function of glutamate receptors by trafficking from the ER, insertion into the plas-

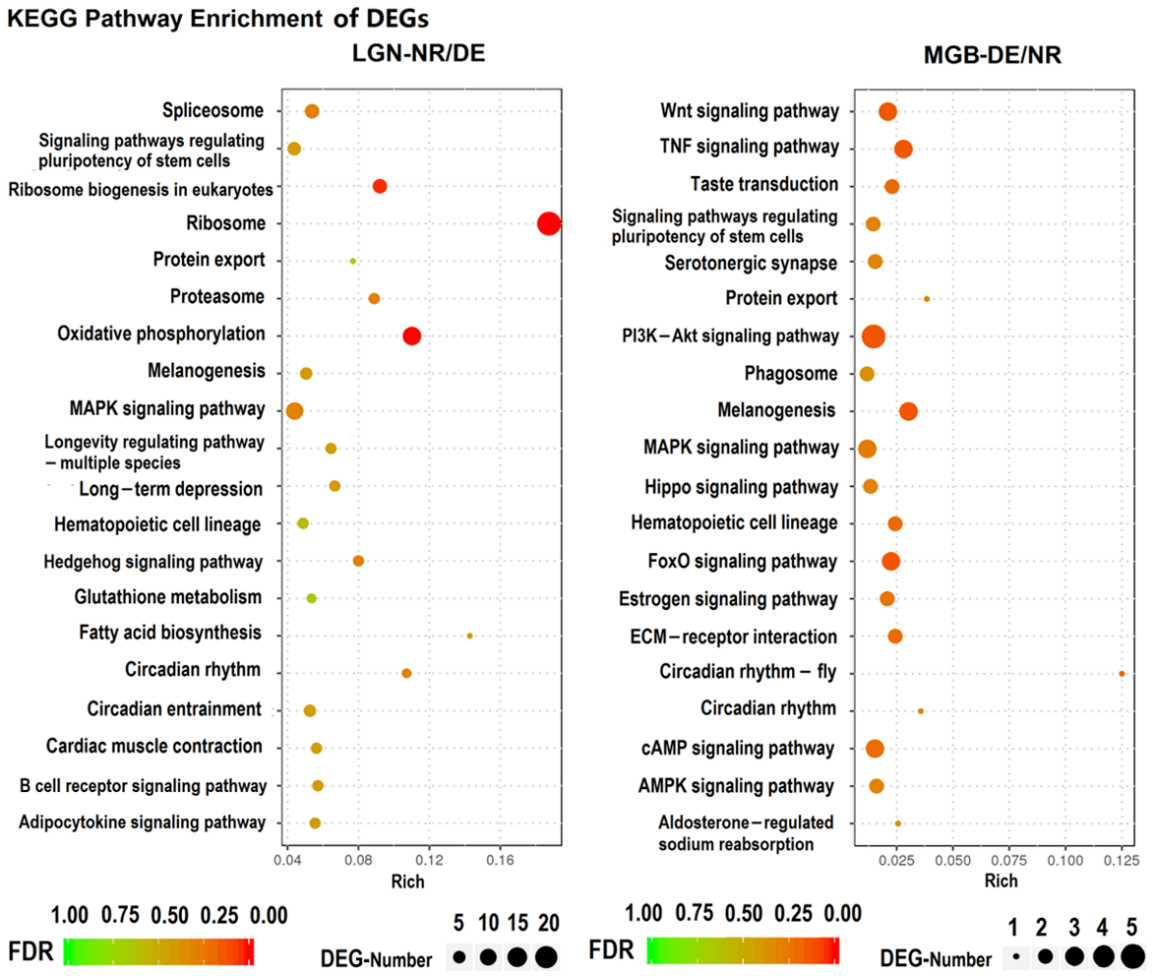

Figure 8. KEGG pathway enrichment analyses of differentially-expressed genes. Left shows the differential expression genes from LGN, right shows the differential expression genes from MGB.

ma membrane, endocytosis, synaptic localization, and binding to other proteins [31]. Previous study has shown that GluR1 expression at the synapse is constant, but the $Serine_{845}$ phosphorylation of GluR1 is able to increase the mEPSCs amplitude in the V1 cortex after visual deprivation [11]. These data strongly imply that the dynamic expression of GluRs and their post-translational phosphorylation are involved in regulating the synaptic plasticity in the primary cortices in the absence of sensory input. In addition, the expression level of NR2B was increased, but that of NR2A in the layer IV of V1 cortex was decreased after DE. The switch from predominantly NR2B to NR2A subtypes is experience-dependent, and visual deprivation can delay the rising tendency of NR2A in the layer IV of V1 cortex [32, 33]. These data provide the underlying molecular component accounting for the increased neural electrical activity in the layer IV of V1 cortex after visual deprivation [17]. In the layer II/III of V1 cortex, the expression levels of GluR1 and GluR2 were constant after DE found in the present study, it is speculated that the above mentioned phosphorylation maybe account for the increased amplitude of AMPA-mediated mEPSCs in the layer II/III of V1 cortex after visual deprivation [11, 15]. The expression level of NR1 in the layer II/III of V1 cortex was obviously increased after DE, which may indicate a novel molecular regulatory element for mediating the enhanced LFP oscillation in the layer II/III of V1 cortex. Furthermore, the present study revealed that the expression levels of GluR1, GluR2, and NR2B were either up- or down-regulated in the layer V and layer VI of V1 cortex after DE, indicating the efferent pathway as well as the intracortical circuit of V1 cortex undergo more extensively embellished after visual deprivation.

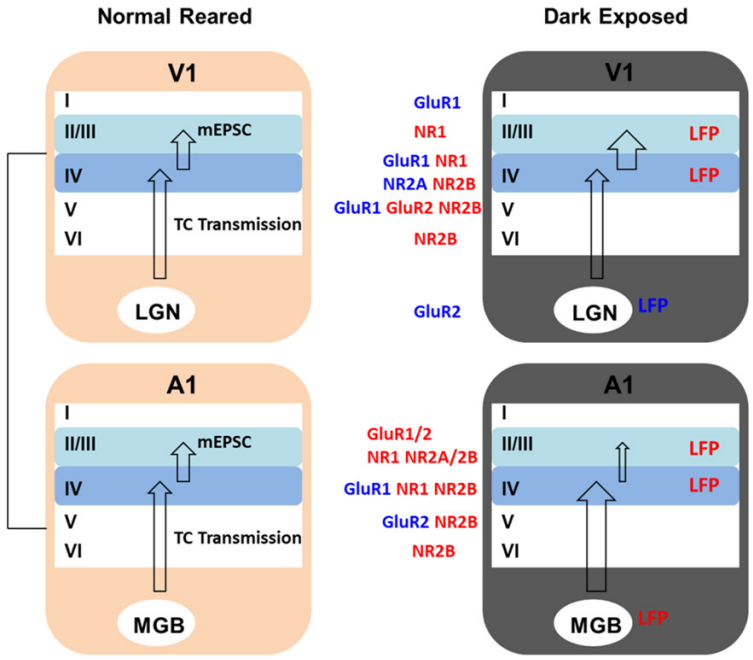

Figure 9. Schema graph illustrating the underlying mechanisms of cross-modal plasticity. Geol et al. (2006) reported that the mESPC amplitude of pyramidal neuron in the layer II/III of V1 cortex was increased and that in the layer II/III of A1 cortex was decreased after DE (black arrow). Petrus et al. (2014) reported that DE strengthened thalamocortical (TC) synapses (projection from MGB to layer IV) in the A1 cortex, but not in the V1 cortex (black arrow). Pan et al. (2018) observed that LFP activities in the layer IV of V1 and A1 cortices and MGB were enhanced, and that in LGN was decreased after DE. The present study verified that LFP activities in the layer II/III of V1 and A1 cortices were enhanced, and the expression levels of five GluR subunits were up-/down-regulated in V1 and A1 cortices with layer-specificity after DE (red symbol signify up-regulation, blue symbol signify down-regulation).

In the layer IV of A1 cortex, the expression level of GluR1, but not that of GluR2 was decreased after DE observed in the present study. It seems to be incorrelate with the increased amplitude of AMPA-mediated mEPSCs in layer IV of the A1 cortex [15], which thus clearly hints the indispensable role of posttranslational modification in shaping GluRs function. In addition, the expression levels of NR1 and NR2B were increased in the layer IV of A1 cortex after DE, which was considered to be the pivotal regulatory factor for the intensive neural electrical activity in the layer IV of A1 cortex induced by visual deprivation [17]. In the layer II/III of A1 cortex, the expression levels of GluR1 and GluR2 were down-regulated after DE. This result is correlated with a decrease in AMPA-mediated mEPSCs amplitude in the layer II/III of A1 cortex after visual deprivation [11]. It was unexpected that the expression levels of NMDAR subunits (NR1, NR2A and NR2B) were both increased in the layer II/III of A1 cortex after DE. Thus, NMDR subunits may be involved in shaping the synaptic plasticity in the layer II/III of A1 cortex by losing of vision modality we regarded. It is noteworthy that the GluR subunits including GluR2 and NR2B were likewise presented with subtle expression changes in layer V or/and layer VI of the A1 cortex after DE. These results indicate the possibility of the refined A1 intracircuit and efferent thalamocortical pathway contributed to the enhancement of auditory perception in the absence of visual input.

The role of thalamic LGN and MGB in the cross-modal plasticity following DE

A growing body of work has shown that subcortical structures (such as the thalamus) may account for the cortical reorganization following the lacking of sensory input [34]. Thalamocortical projections from MGB to A1 cortex but not from LGN to V1 cortex are strengthened after visual deprivation [15]. Our previous study observed that LFP activity in the LGN was weakened, which may be attributed to the shirking of the responsibility for processing visual information in the absence of visual input [17]. The present study revealed that 380 genes were either up- or down-regulated, which manifests that transcriptional processes in the LGN remain active, possibly ascribing to the stress reaction induced by lacking of visual input. There is no doubt that MGB is involved in the cross-modal plasticity following visual deprivation [17]. However, only 46 genes involving in PI3K-Akt, Wnt and TNF signal pathways were found to be either up- or down-regulated in the MGB after DE in the present study. These results suggest that signal pathway integration is worthwhile to be approached for deciphering the cross-modal plasticity. In addition, GluR2 was detected to be down-regulated in the LGN after DE, which indicated that GluR2 may be an elicitor

for down-regulated neural activity in the LGN. There was no detected adjustment of GluRs expression in MGB after DE, it was speculated that the posttranslational modification such as phosphorylation of GluRs may be involved in mediating the synaptic plasticity in MGB after DE.

Conclusions

The present study demonstrated the layer-specific expression variation of five GluR subunits in visual and auditory primary cortices following visual deprivation. The fruits made in the study may allow us to reach a conclusion that the GluRs regulation is a common downstream mechanism for global homeostatic plasticity in sensory primary cortices in the absence of visual input.

Acknowledgements

This study was supported by the National Natural Science Foundation of China (3157-1032, 81900930, and 81730028), the Key Research and Development Program of the Ministry of science and technology of China (SQ2017YFSF080012), and the China Postdoctoral Science Foundation (2018M640407).

Disclosure of conflict of interest

None.

Address correspondence to: Yonghua Ji, Institute of Biomembrane and Biopharmaceutics, Shanghai University, 333 Nanchen Road, Baoshan District, Shanghai, China. Tel: +86-021-66135189; Fax: +86-021-66135189; E-mail: yhji@staff.shu.edu.cn; Hao Wu, Department of Otorhinolaryngology Head and Neck Surgery, Shanghai Ninth People's Hospital, School of Medicine, Shanghai Jiao Tong University, Shanghai, China; Laboratory of Auditory Neuroscience, Ear Institute, School of Medicine, Shanghai Jiao Tong University, Shanghai, China; Shanghai Key Laboratory of Translational Medicine on Ear and Nose Diseases, 115 Jinzun Road, Pudong District, Shanghai, China. Tel: +86-021-38452258; Fax: +86-021-38452258; E-mail: haowu@sh-jei.org

References

[1] Goldreich D and Kanics IM. Tactile acuity is enhanced in blindness. J Neurosci 2003; 23: 3439-3445.

[2] Lessard N, Pare M, Lepore F and Lassonde M. Early-blind human subjects localize sound sources better than sighted subjects. Nature 1998; 395: 278-280.

[3] Roder B, Teder-Salejarvi W, Sterr A, Rosler F, Hillyard SA and Neville HJ. Improved auditory spatial tuning in blind humans. Nature 1999; 400: 162-166.

[4] Gougoux F, Lepore F, Lassonde M, Voss P, Zatorre RJ and Belin P. Neuropsychology: pitch discrimination in the early blind. Nature 2004; 430: 309.

[5] Beaulieu-Lefebvre M, Schneider FC, Kupers R and Ptito M. Odor perception and odor awareness in congenital blindness. Brain Res Bull 2011; 84: 206-209.

[6] Zhou Y, Fang FH, Pan P, Liu ZR and Ji YH. Visual deprivation induce cross-modal enhancement of olfactory perception. Biochem Biophys Res Commun 2017; 486: 833-838.

[7] Cohen LG, Celnik P, Pascual-Leone A, Corwell B, Falz L, Dambrosia J, Honda M, Sadato N, Gerloff C, Catala MD and Hallett M. Functional relevance of cross-modal plasticity in blind humans. Nature 1997; 389: 180-183.

[8] He K, Petrus E, Gammon N and Lee HK. Distinct sensory requirements for unimodal and cross-modal homeostatic synaptic plasticity. J Neurosci 2012; 32: 8469-8474.

[9] Sterr A, Muller MM, Elbert T, Rockstroh B, Pantev C and Taub E. Perceptual correlates of changes in cortical representation of fingers in blind multifinger Braille readers. J Neurosci 1998; 18: 4417-4423.

[10] Mountcastle VB. The columnar organization of the neocortex. Brain 1997; 120: 701-722.

[11] Goel A, Jiang B, Xu LW, Song L, Kirkwood A and Lee HK. Cross-modal regulation of synaptic AMPA receptors in primary sensory cortices by visual experience. Nat Neurosci 2006; 9: 1001-1003.

[12] Nys J, Aerts J, Ytebrouck E, Vreysen S, Laeremans A and Arckens L. The cross-modal aspect of mouse visual cortex plasticity induced by monocular enucleation is age dependent. J Comp Neurol 2014; 522: 950-970.

[13] Van Brussel L, Gerits A and Arckens L. Evidence for cross-modal plasticity in adult mouse visual cortex following monocular enucleation. Cereb Cortex 2011; 21: 2133-2146.

[14] Petrus E, Rodriguez G, Patterson R, Connor B, Kanold PO and Lee HK. Vision loss shifts the balance of feedforward and intracortical circuits in opposite directions in mouse primary auditory and visual cortices. J Neurosci 2015; 35: 8790-8801.

[15] Petrus E, Isaiah A, Jones AP, Li D, Wang H, Lee HK and Kanold PO. Crossmodal induction of thalamocortical potentiation leads to enhanced information processing in the auditory cortex. Neuron 2014; 81: 664-673.

[16] Traynelis SF, Wollmuth LP, McBain CJ, Menniti FS, Vance KM, Ogden KK, Hansen KB, Yuan H, Myers SJ and Dingledine R. Glutamate receptor ion channels: structure, regulation, and function. Pharmacol Rev 2010; 62: 405-496.
[17] Pan P, Zhou Y, Fang F, Zhang G and Ji Y. Visual deprivation modifies oscillatory activity in visual and auditory centers. Animal Cells Syst (Seoul) 2018; 22: 149-156.
[18] David FO, Hugues E, Cenier T, Fourcaud-Trocme N and Buonviso N. Specific entrainment of mitral cells during gamma oscillation in the rat olfactory bulb. PLoS Comput Biol 2009; 5: e1000551.
[19] Brunet N, Bosman CA, Roberts M, Oostenveld R, Womelsdorf T, De Weerd P and Fries P. Visual cortical gamma-band activity during free viewing of natural images. Cereb Cortex 2015; 25: 918-926.
[20] Schmiedt JT, Maier A, Fries P, Saunders RC, Leopold DA and Schmid MC. Beta oscillation dynamics in extrastriate cortex after removal of primary visual cortex. J Neurosci 2014; 34: 11857-11864.
[21] Ahmad M, Polepalli JS, Goswami D, Yang X, Kaeser-Woo YJ, Sudhof TC and Malenka RC. Postsynaptic complexin controls AMPA receptor exocytosis during LTP. Neuron 2012; 73: 260-267.
[22] Beattie EC, Carroll RC, Yu X, Morishita W, Yasuda H, von Zastrow M and Malenka RC. Regulation of AMPA receptor endocytosis by a signaling mechanism shared with LTD. Nat Neurosci 2000; 3: 1291-1300.
[23] Wenthold RJ, Petralia RS, Blahos J II and Niedzielski AS. Evidence for multiple AMPA receptor complexes in hippocampal CA1/CA2 neurons. J Neurosci 1996; 16: 1982-1989.
[24] McBain CJ and Mayer ML. N-methyl-D-aspartic acid receptor structure and function. Physiol Rev 1994; 74: 723-760.
[25] Monyer H, Burnashev N, Laurie DJ, Sakmann B and Seeburg PH. Developmental and regional expression in the rat brain and functional properties of four NMDA receptors. Neuron 1994; 12: 529-540.
[26] Chen WS and Bear MF. Activity-dependent regulation of NR2B translation contributes to metaplasticity in mouse visual cortex. Neuropharmacology 2007; 52: 200-214.
[27] Yashiro K, Corlew R and Philpot BD. Visual deprivation modifies both presynaptic glutamate release and the composition of perisynaptic/extrasynaptic NMDA receptors in adult visual cortex. J Neurosci 2005; 25: 11684-11692.
[28] Raizada RD and Grossberg S. Towards a theory of the laminar architecture of cerebral cortex: computational clues from the visual system. Cereb Cortex 2003; 13: 100-113.
[29] Wagstyl K, Lepage C, Bludau S, Zilles K, Fletcher PC, Amunts K and Evans AC. Mapping cortical laminar structure in the 3D BigBrain. Cereb Cortex 2018; 28: 2551-2562.
[30] Constantinople CM and Bruno RM. Deep cortical layers are activated directly by thalamus. Science 2013; 340: 1591-1594.
[31] Malinow R and Malenka RC. AMPA receptor trafficking and synaptic plasticity. Annu Rev Neurosci 2002; 25: 103-126.
[32] Cho KK, Khibnik L, Philpot BD and Bear MF. The ratio of NR2A/B NMDA receptor subunits determines the qualities of ocular dominance plasticity in visual cortex. Proc Natl Acad Sci U S A 2009; 106: 5377-5382.
[33] Philpot BD, Sekhar AK, Shouval HZ and Bear MF. Visual experience and deprivation bidirectionally modify the composition and function of NMDA receptors in visual cortex. Neuron 2001; 29: 157-169.
[34] Voss P, Collignon O, Lassonde M and Lepore F. Adaptation to sensory loss. Wiley Interdiscip Rev Cogn Sci 2010; 1: 308-328.

Materials and methods

Nissl staining

Laminar architecture of the mouse primary cortex was performed using Nissl staining in the present study. The mouse brain coronal sections (16 μm) from NR group (this procedure is same to that of immumohistochemical staining) were placed in the Cresyl violet Stain (G1430; Solarbio, Beijing, China) at 56°C for 1 h. Then, the sections were rinsed with distilled water and placed in the Nissl Differentiation (G1430; Solarbio) for 2 min. Finally, the sections were soaked in absolute ethyl alcohol, immersed in xylene, sealed with neutral balsam, and photographed using an upright microscope (Nikon, Sendai, Japan).

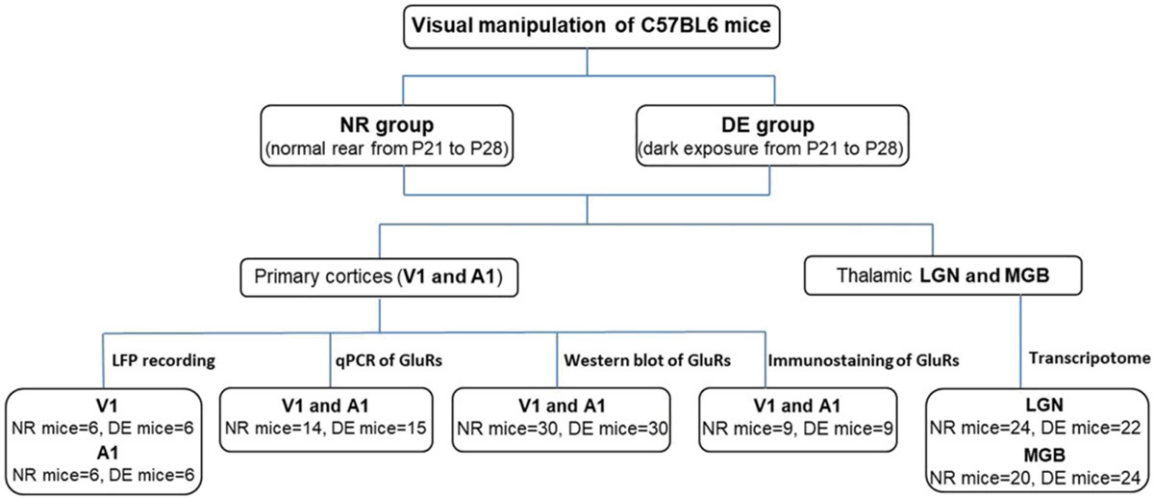

Figure S1. Schematic outline of the experimental protocol used in this study.

Table S1. The primers of mouse GluR subunits for quantitative qPCR

Name	Direction	Sequence (5'-3')	Length (bp)
GluR1	S	TCTAACAACCACGGAGGAAGGAT	158
	A	AGGATGTAGTGGTACCCGATGC	
GluR2	S	TGGAGCACACACAGCGACAAT	182
	A	GCCCTTTCTATTTCCACGCCT	
NR1	S	GCAGATGGCAAGTTTGGCAC	169
	A	TGGTACTTGAAGGGCTTGGAGA	
NR2A	S	CTCTTCTCCATCAGCAGGGG	180
	A	TTTTGGGTGAGTCCATTCGC	
NR2B	S	CTCCACCACCAAGTATCCTCAA	153
	A	CTTGTCTTTCAGGCTCACGCT	
β-actin	S	GGCTGTATTCCCCTCCATCG	154
	A	CCAGTTGGTAACAATGCCATGT	

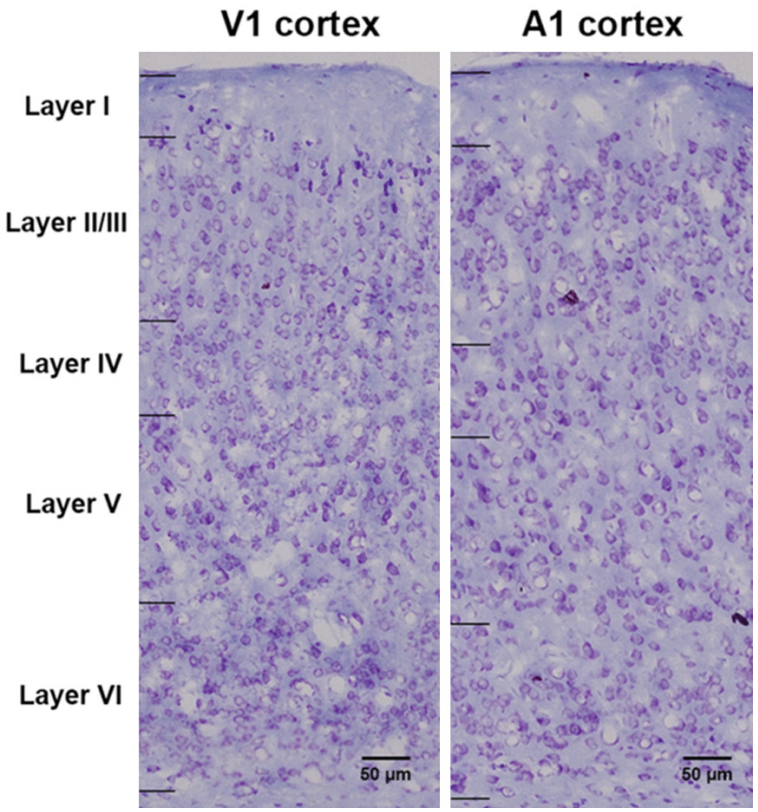

Figure S2. Nissl staining of the mouse V1 and A1 cortices. The V1 and A1 regions can be divided into five layers (Layer I, II/III, IV, V, and VI) according to the laminar architecture in the neocortex. Scale bar: 50 μm.

Table S2. The summary of transcriptome sequence analysis

Sample	Sequencing Mode	Clean Data (bp)	Clean Reads	Q20 (%)	Q30 (%)
NR-LGN-1	Paired-end 2 × 150 bp	6,209,657,674	42,304,430	98.47	95.70
NR-LGN-2		6,008,255,906	40,943,828	98.44	95.60
DE-LGN-1		6,128,505,984	41,739,998	98.40	95.60
DE-LGN-2		6,487,895,438	44,208,720	98.50	95.80
NR-MGB-1		6,762,340,116	45,413,076	97.67	94.34
NR-MGB-2		6,562,437,128	44,065,356	97.78	94.56
DE-MGB-1		6,693,542,434	44,938,156	97.69	94.35
DE-MGB-2		6,658,351,348	44,705,950	97.49	93.90

NR-LGN-1 and NR-LGN-2: the LGN samples of NR group (two independent biological replicates). DE-LGN-1 and DE-LGN-2: the LGN samples of DE group. NR-MGB-1 and NR-MGB-2: the MGB samples of NR group. DE-MGB-1 and DE-MGB-2: the MGB samples of DE group. Q20: The percentage of bases with a Phred value >20. Q30: The percentage of bases with a Phred value >30.